Capillary-Assisted Evaporation of Water from Finned Tubes – Impacts of Experimental Setups and Dynamics

Jan Seiler[*,1], *Rahel Volmer*[*,2], *Dennis Krakau*[1], *Julien Pöhls*[2], *Franziska Ossenkopp*[2], *Lena Schnabel*[2] *and André Bardow*[1,3]

* both authors contributed equally to the publication

[1] RWTH Aachen University, Institute of Technical Thermodynamics
[2] Fraunhofer Institute for Solar Energy Systems ISE, Department Heating and Cooling Technologies
[3] Forschungszentrum Jülich, Institute of Energy and Climate Research, Energy Systems Engineering (IEK-10)

Corresponding author **at all stages of refereeing until publication is final**
Jan Seiler, M.Sc.
Fax: +49 241 80-92255
Tel: +49 241 80-98177
Email: Jan.Seiler@ltt.rwth-aachen.de

Corresponding authors **for final publication and post-publication (names have to be on the final publication as corresponding authors)**

Prof. Dr.-Ing. André Bardow
Fax: +49 241 80-922552
Tel: +49 241 80-95380
Email: Andre.Bardow@ltt.rwth-aachen.de

Rahel Volmer
Tel: +49 761 4588-2018
Email: Rahel.Volmer@ise.fraunhofer.de

Keywords:

Thin-film evaporation; natural refrigerant water (R-718); capillary action; filling level; finned copper tube; adsorption heat pump / chiller

Abstract

Capillary-assisted thin-film evaporation is a promising approach to overcome the heat transfer challenges associated with sub-atmospheric evaporation of water in refrigeration applications. Consequently, thin-film evaporation is currently studied in several labs. However, so far it has been unclear whether results from different labs can be compared. In this work, we therefore investigate - for the first time - the impact of experimental setups and procedures on sub-atmospheric capillary-assisted thin-film evaporation of the refrigerant water and deduce methodological recommendations for improving reliability and comparability of measurement results. We present results of evaporation from finned copper tubes with decreasing filling levels from two different experimental setups:
At higher driving force, the resulting dynamics of logarithmic mean temperature differences, heat flows and overall heat transfer coefficients determined in both setups are generally in good agreement but absolute values show deviations of up to 24 %. For lower driving forces, the results are identical within uncertainty of measurement. We conclude that the impact of experimental setup is important when comparing absolute values from different setups, but obtaining comparable results is generally possible.
Furthermore, we compare experiments with continuously decreasing versus constant filling levels and show that both procedures yield the same results within measurement uncertainty. With decreasing filling level, however, overall heat transfer coefficients are systematically 5-10% higher. Thus, experiments with continuously decreasing filling level are well-suited for a fast analysis of all filling levels in a single experiment.

Nomenclature

Latin letters

A	reference surface area
CV	coefficient of variation
d_o	diameter of tube (from fin tip to fin tip)
f	function
f_{rel}	relative filling level (cf. Fig.2)
h	specific enthalpy
i	control variable
k	coverage factor for expanded uncertainty, used in GUM
L	length
n	number of tubes
p	pressure
$\dot{Q}$	heat flow
Re	Reynolds number
t	timestep
T	temperature
ΔT_{ln}	logarithmic mean temperature difference
u	uncertainty
U	overall heat transfer coefficient
y	variable
$\dot{V}$	volume flow
x_i	uncorrelated input quantities

Greek symbols

Δ	difference
ρ	density

Subscripts

in	inlet
ln	logarithmic
out	outlet
rel	relative
sat	saturation
v	vapour
0	start

Abbreviations

BMWi	Bundesministerium für Wirtschaft und Energie
CAD	computer aided design
Cu	copper
fpi	fins per inch
GUM	Guide to the Expression of Uncertainty in Measurement
highDF	high driving force
IAPWS	International Association for the Properties of Water and Steam
ISE	Fraunhofer Institute for Solar Energy Systems
ISO-KF	vacuum-tight ISO standard quick release flange
lowDF	low driving force

NIST	National Institute of Standards and Technology
PMMA	Poly(methyl methacrylate)
Pt100	platinum resistance thermometer with a resistance of 100 Ω at 0 °C
R-718	refrigerant water (ASHRAE Number)
RefProp	NIST Reference Fluid Thermodynamic and Transport Properties Database
RWTH	Rheinisch Westfälische Technische Hochschule Aachen
SI	Supplementary Information

1 Introduction

Using water as natural refrigerant in heat transformation has many advantages: Water is environmentally friendly, absolutely safe (e.g. non-hazardous) and offers a high enthalpy of vaporization. However, efficient evaporation of water is challenging at low temperatures as nucleate boiling occurs at these temperatures only at high superheats [1]. High superheats are required for pool boiling since the hydrostatic pressure of the water column above the heat exchanger is in the same order of magnitude as the saturation pressure (almost vacuum condition, e.g. 12 mbar at 10 °C). Thus, the local saturation temperature at the submerged heat exchanger surface is increased and consequently higher wall temperatures are necessary to induce nucleate boiling [1]. As high superheats would reduce the cycle efficiency, nucleate boiling is not practical for efficient evaporation of water at low temperatures.

To efficiently evaporate water at low temperatures, the height of the water column can be reduced until only a thin film with low thermal resistance is left: Thin-film evaporation has been shown to offer high heat transfer coefficients [2] with small required superheats [3].

State-of-the-art evaporators for thin- film evaporation are falling-film evaporators, e.g. plain tube bundles sprinkled with refrigerant to create a thin film [4,5]. Falling-film evaporators work well but require a refrigerant pump. However, refrigerant pumps are often undesirable since they include moving parts inside their vacuum shell, need to be protected against cavitation and require auxiliary energy.

Alternatively, the thin film on the heat exchanger can be created by capillary action. Capillary action can be provided by different structures such as fin-and-tube heat exchangers [6–8], plate fin heat exchangers [9,10], finned tubes [11], micro structures [12], coatings [13] and (macro) porous structures [9,10,14].

Besides different structures, the following aspects of capillary-assisted thin-film evaporation of water have been discussed in literature: (I) evaporation temperature, (II) driving force (the potential difference that causes evaporation , most commonly expressed as a temperature difference) and (III) filling level, i.e., the degree to which the heat exchanger is submerged in refrigerant.

I. Higher evaporation temperatures (and thus higher saturation pressure) increase heat transfer coefficients due to changed physical properties of the refrigerant [3,11,13,15].
II. The impact of driving force on thin-film evaporation is not consistently described in literature which suggests that its effect might depend on particular evaporating structures and operational conditions. Xia et al. [11] report a decrease of the heat transfer coefficient with increasing driving force whereas Volmer et al. [6] and Lanzerath et al. [13] detected no impact under the considered conditions. Recently, measurements of Seiler et al. [3] showed no impact of driving force on thin-film evaporation as long as no dry-out of the thin film occurred.
III. The filling level directly affects the area available for thin-film evaporation on the heat exchanger. Thus, as long as no dry-out occurs, the heat transfer coefficient increases with lower filling levels as more area is available for thin-film evaporation [3,11,13].

Unfortunately, many results reported in literature cannot be directly compared due to differences in evaporator type and experimental parameters, such as (I) evaporation temperature, (II) driving force and (III) filling level. Importantly, the impact of employed experimental setups and procedures on sub-atmospheric thin-film evaporation of water has – to the best of our knowledge - not been analysed. However, our measurement experience suggests that also these “hidden” factors linked to experimental setup and procedure can potentially have a large impact on the experimental results – but can easily be missed in measurement evaluation: E.g., non-condensable gases intruding the vacuum system can influence condensation [16] and evaporation [17] and distort vapour pressure measurements. Consequently, the validity, repeatability and comparability of published measurement results can often not be ensured today.

Therefore, the first objective of this work is to fill this gap by identifying and discussing potential impacts due to setups and procedures on thin-film evaporation measurements. On that basis, we want to disclose which steps are necessary to realize comparable and reproducible evaporator characterization. For this purpose, we investigate a set of identical tubes at the same experimental parameters in two different experimental setups. As the main evaluation quantity, we use the overall heat transfer coefficient U which allows the highest possible generalisation. In both setups, measurements are conducted with decreasing filling level since this type of measurement offers the advantage of including all possible filling levels in one single experiment. However, these dynamic experiments create only quasi-steady-state conditions whose impact on the evaporation process has not yet been determined.
Therefore, as a second objective, we assess the comparability of experiments with decreasing filling level and with constant filling levels.
We used two different experimental setups located at two different locations: One experimental setup is located in a lab at the Institute of Technical Thermodynamics at RWTH Aachen University, Germany (from now on referred to as RWTH) and the other experimental setup is located in a lab at the Fraunhofer Institute for Solar Energy Systems ISE in Freiburg, Germany (from now on referred to as ISE). The experimental setups were operated by the authors according to their affiliation stated above.
From our experimental findings, we deduce methodological recommendations to contribute to good scientific practice for improving reliability and comparability of measurement results for sub-atmospheric thin-film evaporation of water.

2 Materials and Methods

2.1 Investigated finned copper tubes

All evaporation measurements were carried out with the natural refrigerant water (R-718) on the same type of finned copper tubes, provided by Wieland-Werke AG. Geometric characteristics of the tubes were chosen in a way that a strong capillary effect and thus high evaporation performance can be expected at the given conditions. An internal structure ensured a high heat transfer on the fluid side. Thus, dynamics in the overall heat transfer coefficient U can be attributed to changes in heat transfer of thin-film evaporation on the refrigerant side. Geometric specifications of the finned tube are listed in Table 1 and a photo of a finned tube installed in the experimental setup at RWTH is given in Fig. 1.

Table 1: Geometric specifications of the finned tube.

Material	Tube inner diameter	Tube outer diameter (fin tips)	Fin spacing	Fin width	Fin height
Cu (C12200)	9.6 mm	13.2 mm	56 fpi	0.15 mm	0.8 mm

The heat exchangers consisted of four identical tubes, which were serially connected (cf. Fig. 2 and Fig. 3). Each tube section has a finned length of 0.5 m which yields a total length of 2 m. The distance between the tube axes is 39 mm. Since measurements were conducted in two different experimental setups, the tube heat exchangers were configured in a slightly different way: For the RWTH setup, the tubes are led through the evaporator chamber walls and interconnected outside the evaporator chamber (Fig. 2 (a) and (b)). For the ISE setup, ”U”-bends are soldered to the tube ends and the whole heat exchanger is installed and connected to the fluid circuit inside the evaporator chamber (Fig. 3).

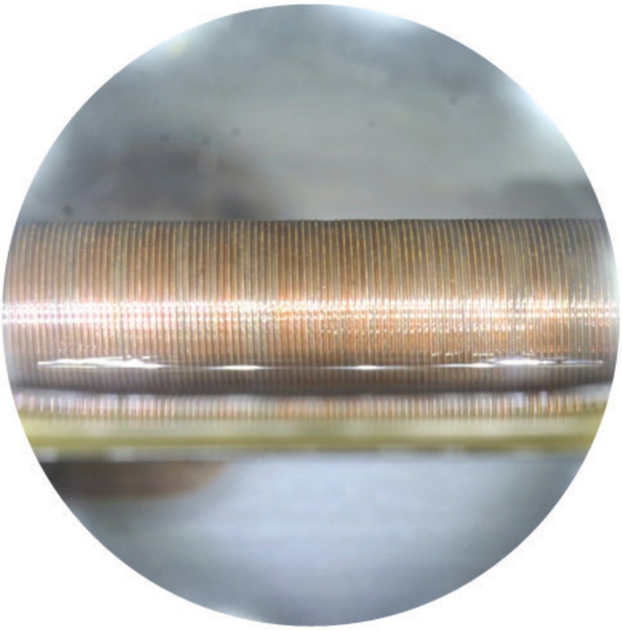

Fig. 1: Finned tube installed in the experimental setup at RWTH partly submerged in the refrigerant water during an experiment. The picture is taken through a round window on the side of the experimental setup. The other three tubes lie behind the shown tube. Capillary water between the fins of the tube as well as the menisci of water at the tube and at the window can be seen.

2.2 Experimental setups

The two experimental setups at RWTH and at ISE had a similar design concept but differed in some aspects:
Both setups consisted of a vacuum-tight system to allow for sub-atmospheric pressure evaporation of the refrigerant water. All materials were chosen such that corrosion-induced formation of non-condensable gases inside the system was avoided. Both setups featured a vacuum chamber, in which evaporation on the finned tubes took place, and a condenser which created the driving force for the evaporation process and which represented a refrigerant reservoir. In the fluid circuits for evaporator and condenser, two thermostats were used to set the volume flow and inlet temperature of the heat transfer fluid water.
The specifics of each setup are pointed out in the following.

2.2.1 Experimental setup RWTH

The evaporator chamber was designed to allow for quick change of the four installed tubes (Fig. 2 (a) and (b)). A condenser consisting of a double helix made from copper tube was used to create the driving force for the evaporation process. As the condenser was located above the evaporator, gravity was used for the refill process of liquid refrigerant into the evaporator (Fig. 2 (b)). The evaporator was directly flooded with the liquid refrigerant up to the desired filling level. The filling level could either decrease during the evaporation experiments by omitting any refilling and keeping the liquid refrigerant in condenser or the filling level could be kept constant by a continuous reflux of the liquid refrigerant from the condenser.

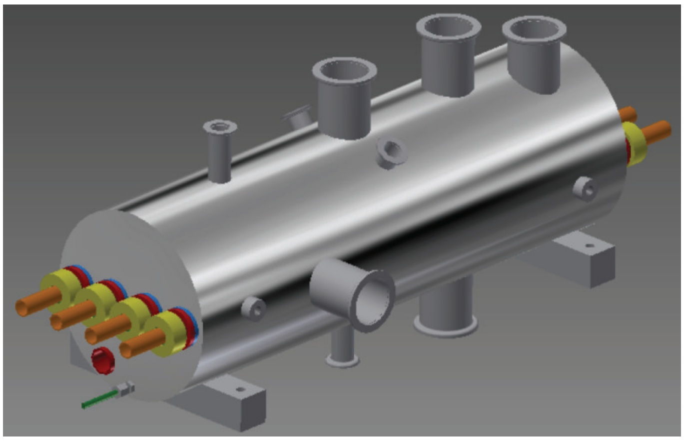

(a)

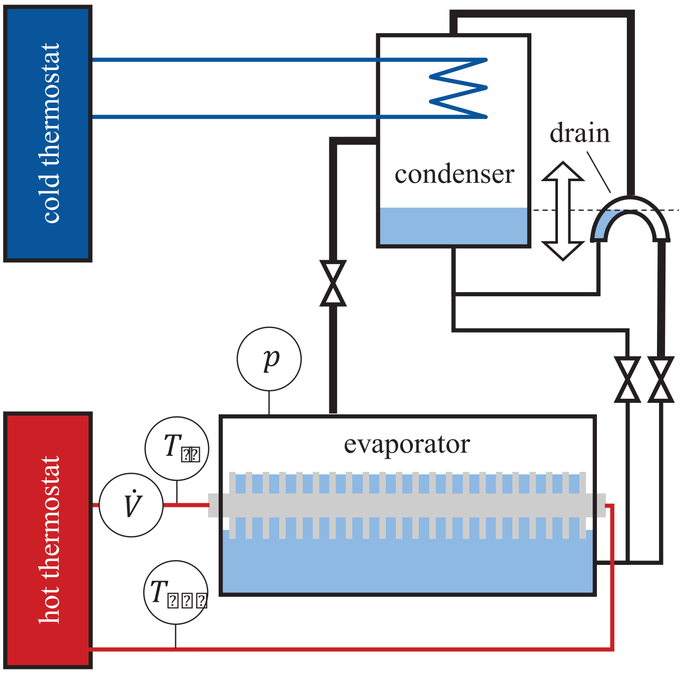

(b)

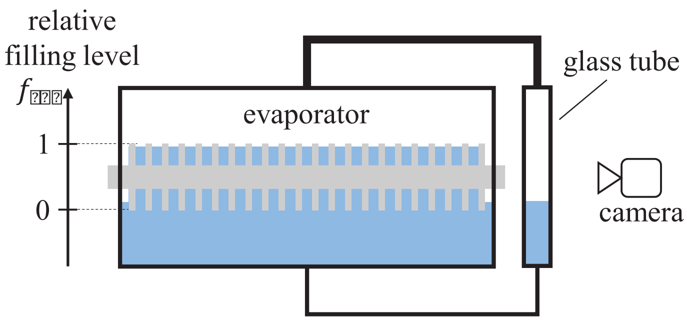

(c)

Fig. 2: Experimental setup at RWTH:
(a) CAD drawing of evaporator chamber with 4 tubes installed. Interconnection of the 4 tubes is outside of the evaporator chamber. ISO-KF flanges are used for sensors, the vacuum pump, windows and liquid / steam connections to condenser and the communicating pipe (cf. (c)).
(b) Sketch of experimental setup consisting of investigated finned tube evaporator with vapour connection to condenser and a mobile level drain for liquid reflux. The setup is shown in side view:

the other three tubes lie behind shown tube. For simplification, in- and outlet are shown on opposite sides of the first tube; in reality, they are on the same side on the first and the last of the four tubes. Capillary water between fins is also shown.
(c) Definition of relative filling level f_{rel} (left) and detection of filling level with communicating pipe (glass tube) in experimental setup at RWTH (right).

To allow for measurements at constant filling level, the experimental setup was equipped with a drain (Fig. 2 (b)). Once the refrigerant in the condenser reaches the level of the drain, any additional condensed refrigerant flows directly back into the evaporator and the filling level in the evaporator is kept constant. The filling level in the evaporator can be decreased by moving the level drain upwards such that more refrigerant is stored in the condenser before the refrigerant reaches the level drain and flows into the evaporator. Correspondingly, by moving the level drain downwards, the filling level in the evaporator is increased.
In this work, the filling level of the evaporator is given as the relative filling level f_{rel} which equals 1 if the filling level is at the top of the tube and 0 if it is at the bottom of the tube as shown in Fig. 2 (c) on the left. Negative filling levels are possible when the filling level is below the tube but capillary forces still maintain a connection between the tube and the water surface by a meniscus.

Detection of the relative filling level f_{rel} in the evaporator proved difficult with standard measuring techniques based on detection of density, capacitance, velocity of sound, etc. since these properties strongly depend on temperature for the considered conditions close to the triple point of water and due to low reliability of available sensors (e.g. effect of water droplets). Instead, we developed an optical system to determine the relative filling level f_{rel} of the refrigerant (Fig. 2 (c), right).

The optical system consisted of a communicating pipe to show the filling level in a glass tube outside the evaporator chamber and a digital camera to capture images of the visible phase interface. The location of the phase interface was determined by a customized self-programmed edge-detection algorithm. Automatic evaluation of 300 pictures per experiment resulted in reliable measurement of the relative filling level f_{rel} (cf. Fig. SI13 in the supplementary information).
The whole experimental setup was automated. Thus, accurate repetitions of the experiments and time-consuming screening of several parameters were possible without active staff support. More details on the experimental setup at RWTH can be found in [3].

2.2.2 Experimental setup ISE

In the experimental setup at ISE (Fig. 3), the evaporator chamber featured integrated hydraulic lead-throughs which allowed installation of various kinds of heat exchangers via vacuum flange connections inside the chamber. The condenser consisted of an over-sized flat tube-fin heat exchanger which was permanently welded into a rectangular vacuum chamber. The condenser heat exchanger was always partially flooded with refrigerant and, thus, served as a refrigerant reservoir while always maintaining a sufficient free surface area for condensation. The evaporation and the condensation chamber were connected by two vapour lines which could be opened or closed by automated valves.

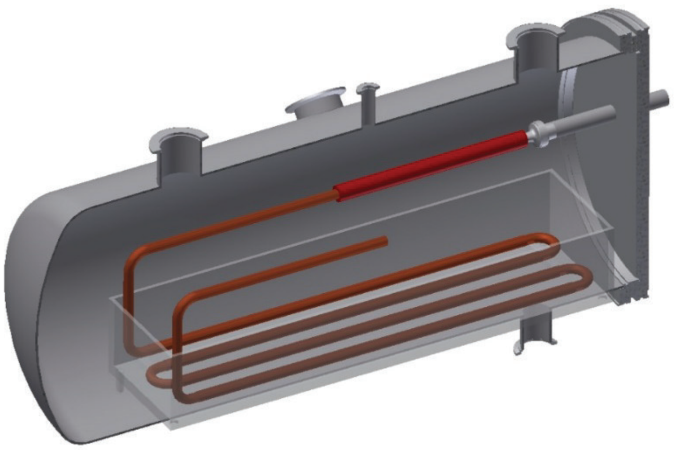

(a)

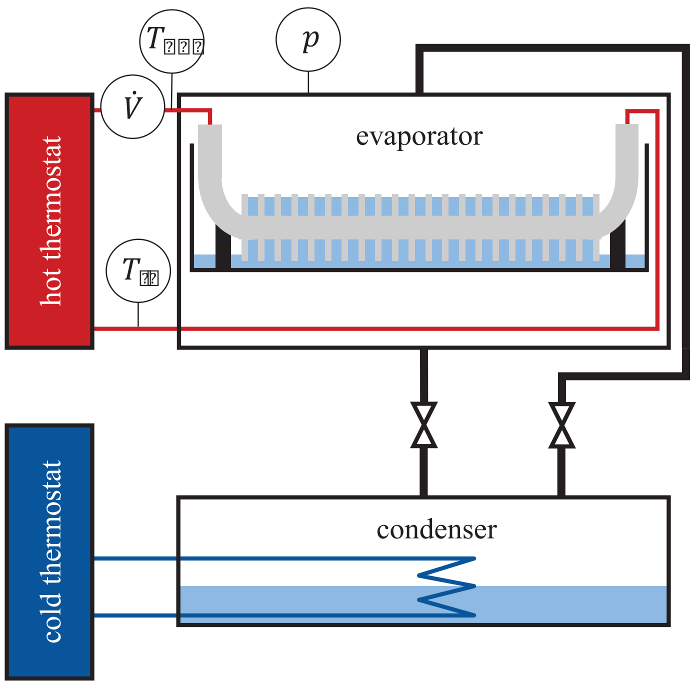

(b)

Fig. 3: Experimental setup at ISE:
(a) CAD drawing of the heat exchanger and trough inside half-section of evaporator chamber in the ISE setup. Interconnection of the 4 tubes is inside the evaporator chamber. ISO-KF flanges are used for sensors, the vacuum pump, windows and steam connections to condenser.
(b) Sketch of experimental setup consisting of investigated finned tube evaporator on two support bars (coloured black in evaporator in figure) in acrylic glass (PMMA) trough placed in an evaporator chamber with vapour connection to the condenser below. The setup is shown in side view: The other three tubes lie behind the shown tube. For simplification, in- and outlet are shown on opposite sides of the first tube; in reality, they are on the same side on the first and the last of the four tubes. Capillary water between fins is also shown.

Since the condenser is placed below the evaporator, refrigerant cannot be fed from the reservoir in the condenser to the evaporator chamber by gravity but by a refrigerant pump (not shown in Fig. 3 (b)) or by condensation on the investigated evaporator. This configuration allows for operational

modes in which excess refrigerant in the evaporator is intended to be drained back to the condenser by gravity. Evaporation can be measured both steady-state and transiently. The measurements described in this work were carried out in transient mode and refrigerant was supplied to the test heat exchanger by condensation.
To obtain comparable time series of measured quantities, it was necessary to ensure that evaporation of a certain amount of refrigerant leads to the same change in filling level in both experimental setups: differences in filling level change would alter the heat transfer rate and thus the time series of all measured quantities. This requirement of equal change in filling level can be realized by creating the same base area in both refrigerant pools. Therefore, at ISE, an open transparent acrylic glass (PMMA) trough with roughly the same base area as the refrigerant pool area at RWTH (0.0812 m^2) was placed inside the evaporation chamber (Fig. 3 (a)). Thus, not the whole evaporator chamber was flooded with refrigerant but only the trough. The finned tube heat exchanger was placed inside the PMMA trough, propped on two support bars of 10 mm height (only the ”U”-bends were in contact with the bars so that the finned tube sections were not blocked), which allowed the refrigerant filling level to drop below the bottom edge of the fins (Fig. 3 (b)) thus creating relative filling levels below 0.

2.3 Data reduction

Both experimental setups measured the same quantities: volume flow $\dot{V}$, in- and outlet temperature T_{in} and T_{out} of the heat transfer fluid inside the evaporator tubes and the pressure p in the evaporator chamber (cf. Fig.2(b) and Fig.3(b)). Thus, we could employ the same data reduction in both cases. Details on the used sensors and thermostats are given in Table 2. For the volume flow sensor and the pressure transducers, we used the calibration provided by the manufacturer. The temperature sensors were calibrated while being connected to the data acquisition of the experimental setups.

Table 2: Experimental equipment: sensors and thermostats. Locations of sensors are given in Fig. 2 (b) and Fig. 3 (b).

Equipment type	**RWTH**			**ISE**		
	manu-facturer	model	uncertainty	manu-facturer	model	uncertainty
Temperature sensor	SE Sensor Electric	Pt100, class A, four wire connection	absolute: 0.02 K in-out: 0.01 K	tmg GmbH	Pt100, class 1/3 B, four wire connection	absolute and in-out: 0.011 K
Pressure transducer	ABB	266AST	0.04 mbar	MKS	Baratron 627B	0.043 mbar
Volume flow sensor	Huba Control	210. 910441K	0.32 l/min	Krohne	Optiflux 1010 C/D + IFC 010 D	0.033 l/min
hot thermostat	Thermo Scientific	P1-C41P	-	Huber	CC-515w	-
cold thermostat	Huber	CC-510w	-	Huber	CC-515w	-

To characterize the heat transfer from the heat transfer fluid through the tubes to the refrigerant vapour phase, we used the overall heat transfer coefficient U

$$U = \frac{\dot{Q}}{A\,\Delta T_{\mathrm{ln}}}, \tag{1}$$

where $\dot{Q}$ is the heat flow from the heat transfer fluid through the reference surface area A of the tubes into the refrigerant on the outside of the tubes. We chose the logarithmic mean temperature difference ΔT_{ln} to describe the driving force for this heat flow.
To determine the heat flow $\dot{Q}$, we applied a steady-state energy balance around the tubes

$$\dot{Q} = \dot{V}\,\rho\,\left(h_{\mathrm{in}}(T_{\mathrm{in}}) - h_{\mathrm{out}}(T_{\mathrm{out}})\right), \tag{2}$$

where $\dot{V}$ is the volume flow of the heat transfer fluid inside the tubes, ρ the density, $h_{\mathrm{in}}(T_{\mathrm{in}})$ and h_{out} (T_{out}) the specific enthalpies of the heat transfer fluid at the in- and outlet of the evaporator tubes. Heat flows from the surroundings into the evaporator were compensated by calibrating the outlet temperature: The required offset was obtained by measuring the difference between in- and outlet temperature in steady-state conditions for the closed evaporator chamber, i.e., every time before the evaporation process started. The determined offsets were in the same order of magnitude as the uncertainty of measurement. The reference surface area A was chosen as the cylindrical surface enclosing the fins to account for the necessary construction volume of the finned tubes. Thus, the diameter d_o (from fin tip to fin tip) and the length L of the investigated n tubes are included in the calculation of A:

$$A = n\,\pi d_o L. \tag{3}$$

The logarithmic mean temperature difference ΔT_{ln} is the driving force and was determined by

$$\Delta T_{\mathrm{ln}} = \frac{T_{\mathrm{in}} - T_{\mathrm{out}}}{\ln\left(\dfrac{T_{\mathrm{in}} - T_{\mathrm{v}}}{T_{\mathrm{out}} - T_{\mathrm{v}}}\right)}. \tag{4}$$

Here, T_{in}, T_{out} and T_{v} are the fluid temperatures at the evaporator in- / outlet and the vapour temperature inside the evaporator chamber. Since direct measurements of the vapour temperature are difficult, we used the saturation temperature of water corresponding to the measured pressure p in the evaporator chamber (assuming absence of non-condensable gases inside the chamber and thermodynamic equilibrium in the vapour phase):

$$T_{\mathrm{v}} = T_{\mathrm{sat}}(p). \tag{5}$$

All needed fluid properties were calculated with TILMedia [18] based on RefProp [19] using the equation of state “IAPWS-95” by [20] fitted among others to data from [21–26].

2.4 Uncertainty in measurement

We calculated measurement uncertainty according to the “Guide to the expression of uncertainty in measurement” (GUM) using a coverage factor of k = 1 [27]. Following the „law of propagation of uncertainty“ for uncorrelated input quantities x_i

$$u_{f(x_i)} = \sqrt{\sum_i \left(\frac{\partial f}{\partial x_i}\right)^2 u_{x_i}^2} \tag{6}$$

where u_{x_i} is the uncertainty of input x_i, we determined the uncertainty $u_{f(x_i)}$ for all quantities used in the data reduction. For our assessment of uncertainty, we accounted for the whole measurement chain including uncertainty of the sensors and data acquisition hardware. Uncertainty in the maximum measured U-value is below 13% for all experiments. Uncertainties for all calculated quantities are given

in Fig. SI9 to Fig. SI12 in the supplementary information (SI). Especially for low heat flows and low driving forces, the uncertainty of the U-value is quite high, particularly due to the uncertainty of the temperature and pressure measurement. Therefore, it is crucial to use temperature and pressure sensors with low measurement uncertainty for this type of experiment.
To assess the consistency of the results from both experimental setups (RWTH and ISE), we use the coefficient of variation *CV* as metric

$$CV = \sqrt{\frac{1}{\mathrm{t}-\mathrm{t}_0}\int_{t_0}^{t}\left(y_{\mathrm{RWTH}} - y_{\mathrm{ISE}}\right)^2 \mathrm{d}t} \Big/ \left(\frac{1}{2}\left(\frac{1}{\mathrm{t}-\mathrm{t}_0}\sum_{i=t_0}^{t} y_{\mathrm{RWTH}}(i) + \frac{1}{\mathrm{t}-\mathrm{t}_0}\sum_{i=t_0}^{t} y_{\mathrm{ISE}}(i)\right)\right) \quad (7)$$

.

The coefficient of variation *CV* relates the root mean square deviation to the mean of both variables y_{RWTH} and y_{ISE} from timestep t_0 to timestep t. A *CV* close to zero shows that the numerical results of both experiments are in good agreement.

2.5 Experimental procedure

Prior to starting the measurement series, the experimental setups were brought to a well-defined state to ensure comparable measurement conditions at both labs (RWTH and ISE).
The heat exchangers were cleaned with isopropanol to remove grease from the production process and installed inside the evaporator chamber.
The evacuated refrigerant reservoirs were sufficiently filled with degassed, deionized / bi-distilled water. After filling, remaining non-condensable gases were thoroughly removed from all system components with a vacuum pump (cf. SI6.3). Additionally, non-condensable gases were removed for each evaporation measurement: In the ISE setup, the condenser and evaporator were evacuated for 4 minutes each, prior to the evaporation. In contrast, in the RWTH setup, the condenser was evacuated through a small aperture plate during the whole experiment to allow for continuous operation of the setup.
Before each evaporation measurement, the heat exchanger tubes were completely flooded with refrigerant so that all surfaces were wetted. Afterwards, all valves connecting evaporator chamber and condenser were closed. Subsequently, the thermostats were set to the target temperatures of the evaporator and condenser fluid inlets. When all components had reached steady-state conditions, the valves (one valve at RWTH, two valves at ISE) between evaporator and condenser chamber were opened to start the evaporation process. In the course of the measurement, the filling level in the evaporator decreased due to evaporation. When the filling level reached the upper edge of the finned tubes, the partially flooded phase started where thin refrigerant films form on the tubes' surfaces due to capillary action in the fin interstices.
For measurements with decreasing filling level, the filling level continuously decreased until the measurements ended when the bottom edges of the tubes lost contact to the refrigerant surface.
For stationary measurements with constant filling level – which were only conducted at RWTH – the level drain (see Fig. 2 (b)) was used to keep the filling level constant at the desired levels. After all measured quantities had reached steady-state conditions (after approximately 30 minutes), the evaporation process was continued for 2 minutes and the quantities measured during these 2 minutes were averaged. Afterwards, the level drain was moved upwards to decrease the filling level to the next constant filling level.

2.6 Input parameters

For comparability of the measurements at RWTH and ISE, input conditions of the experiments need to be identical. The input conditions of the described experiments are: evaporator inlet temperature, volume flow and pressure. Thermostats were used to ensure constant and identical volume flow and inlet temperature in the evaporator (Table 3). The temperature settings adjust both the driving force of the evaporation process and the evaporation temperature (which is associated with the

evaporator pressure). Ideally, the evaporation pressure should also be constant. However, keeping the evaporation pressure constant would require a rather complex control strategy of the experimental setup since fluid inlet temperatures would have to be controlled dynamically by the thermostats. Such a control strategy was not implemented at either of the two locations. Therefore, the condenser inlet conditions were set to obtain comparable evaporation pressures in both experimental setups. As the evaporation pressure was not constant during the experiments, the minimum and maximum values are given in Table 3.
To investigate the impact of driving force, measurements were performed with two pressure ranges in the evaporator with the same fluid inlet temperature leading to an experiment with low driving force (lowDF) and an experiment with high driving force (highDF). The corresponding settings are given in Table 3. Each experiment was repeated at least once in each setup (RWTH and ISE) to guarantee reproducibility of the results.

Table 3: Input parameters for the comparison of experimental setups at RWTH and ISE.

Para-meter set	**Experi-mental setup**	**Evaporator inlet temp-erature**	**Evapo-rator volume flow**	**Evapo-rator inlet *Re***	**Min. evapo-rator pressure**	**Max. evapo-rator pressure**	**Filling level**
low Driving Force: lowDF	RWTH	15 °C	7.9 l/min	1.53 x10^4	15.7 mbar	16.4 mbar	continuously decreasing
	ISE	15 °C	7.9 l/min	1.53 x10^4	15.7 mbar	16.4 mbar	continuously decreasing
high Driving Force: highDF	RWTH	15 °C	7.9 l/min	1.53 x10^4	10 mbar	13.3 mbar	continuously decreasing
	ISE	15 °C	7.9 l/min	1.53 x10^4	10 mbar	13.1 mbar	continuously decreasing

The stationary measurements were carried out at 6 constant filling levels f_{rel} which covered a range from approximately 0.75 to -0.3. For comparison, the measurements were also conducted with decreasing filling level. Further settings for these measurements are given in Table 4. Each measurement was performed at least three times to guarantee reproducibility.

Table 4: Input parameters for comparison of continuously decreasing filling level with constant filling levels.

Parameter set	**Experi-mental setup**	**Evaporator inlet temp-erature**	**Evapo-rator volume flow**	**Evapo-rator inlet *Re***	**Min. evapo-rator pressure**	**Max. evapo-rator pressure**	**Filling level**
Decreasing filling level	RWTH	15 °C	11.0 l/min	2.13 x10^4	13.1 mbar	15.1 mbar	continuously decreasing
Constant filling level	RWTH	15 °C	11.0 l/min	2.13 x10^4	14.1 mbar	15.1 mbar	constant at 6 different levels

3 Results and discussion

3.1 Impact of experimental setups

The discussion is divided in three parts: Comparison of the input quantities, description of the dynamics of the output quantities and comparison of the output quantities.

3.1.1 Comparison of input quantities

Measured input conditions of experiments are shown in the Supplementary Information (SI) (Fig. SI7 and Fig. SI8) for both measurement parameter sets and experimental setups. During thin-film evaporation until the contact between the tubes and the water is lost, the input conditions of both setups show good agreement within uncertainty of measurement. Evaporator volume flow and inlet temperature are constant and almost identical. The evaporator pressure dynamically adapts to current U-values of the evaporator and condenser since no control strategy for keeping the pressure constant was implemented. The resulting shapes and absolute values of the evaporator pressure curve coincide within the uncertainty of measurement for both setups and parameter sets in the relevant period of the experiments. Thus, the prerequisite for comparing the measurements is fulfilled.

3.1.2 Dynamics of output quantities

Resulting values for driving force ΔT_{ln}, heat flow $\dot{Q}$ and overall heat transfer coefficient U are nearly constant at the beginning of the experiment (flooded phase) (Fig. 4 and Fig. 5). When thin-film evaporation starts (partially flooded phase), the driving force ΔT_{ln} at first decreases strongly (heat flow $\dot{Q}$ increases strongly); with decreasing filling level, the curves become less steep. The reason for these dynamics is as follows: In the flooded phase, the thermal resistance and available surface for evaporation are nearly constant; during thin film evaporation, the thermal resistance becomes smaller and the area covered with thin-film surface gradually increases which increases evaporation heat flow $\dot{Q}$. Due to the circular shape of the tube cross-section, the gain in thin-film surface increases fast in the first phase of thin-film evaporation while the gain becomes smaller when the filling level approaches the half height of the tube. As evaporation power increases, the system pressure p (and thus saturation temperature) increases while the evaporator outlet temperature decreases which results in a decrease of the driving force ΔT_{ln}. Decreasing slope of evaporation heat flow $\dot{Q}$ and increasing slope of driving force ΔT_{ln} mostly compensate each other in the calculation of the U-value which results in a virtually linear increase of the U-value over time. The linear increase in U-value is mainly due to an increase in available surface area for thin-film evaporation, as the reference surface area A of the tubes used to calculate the U-value (cf. Eq.(1)) is constant and does not change according to the actually available thin-film surface area for the heat transfer [13].
Thus, the maximum peak of the U–value is located at the end of the experiment, shortly before the contact between the tubes and the refrigerant pool is lost. The detachment of the refrigerant pool from the tube happens at relative filling levels f_{rel} well below 0 since a meniscus continues to connect the tubes to the refrigerant pool even if the pool level is below the tube. The detachment occurs separately for all four tubes which can be seen in four distinctive drops of the U-value at the end of the experiment. Shortly before each drop in U-value, the U-value strongly increases. This increase in U-value is caused by an increase of available surface area: the area which was previously occupied by the meniscus connecting the refrigerant pool to the tube is now made available for thin-film evaporation by the detachment.
The comparison of different experiments should, however, be based on the maximum U-values measured before the contact to the refrigerant is lost, since this operating point can reliably be detected. In practice, relative filling levels f_{rel} above 0 will most likely be chosen for continuous operation to ensure a reliable connection between refrigerant and the tube.
Measured maximum U-values for parameter sets lowDF and highDF in both experimental setups for driving forces ΔT_{ln} from 0.4 K to 1.3 K are quite high ranging from approximately 5.2 kW/m^2/K to 6.8 kW/m^2/K (Fig. 4 and Fig. 5).

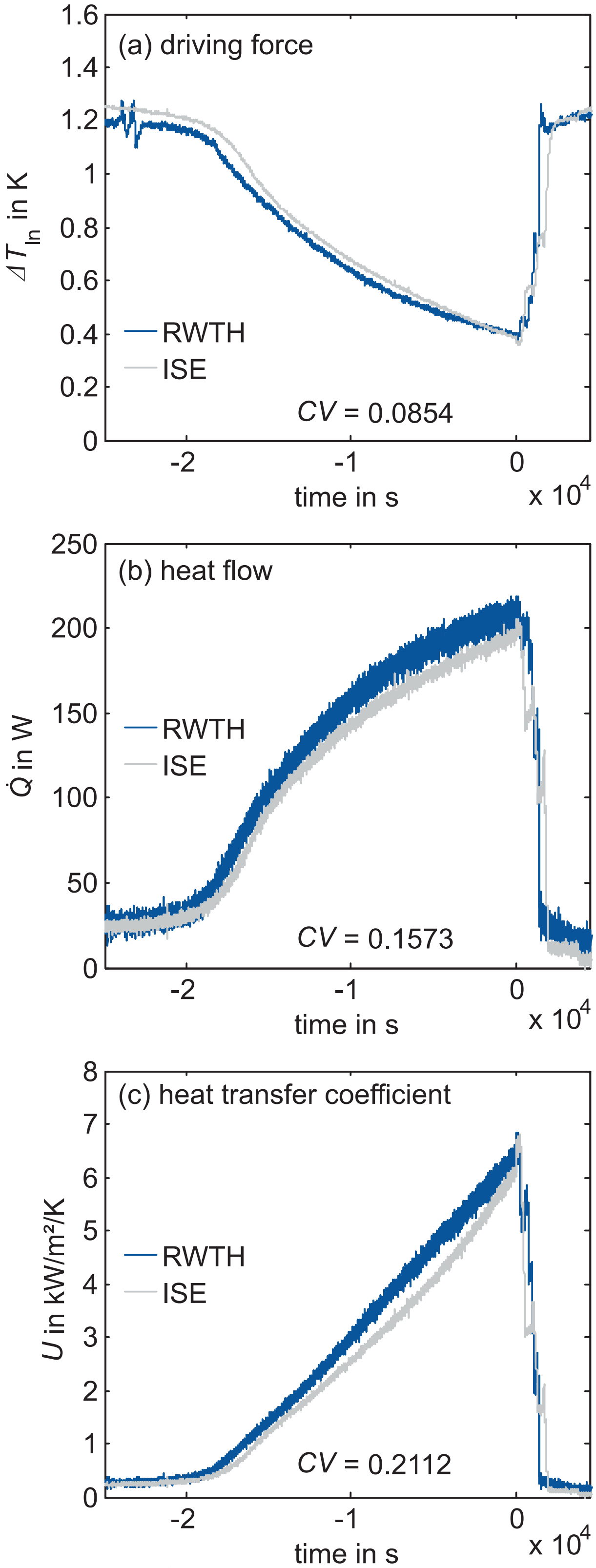

Fig. 4: Driving force ΔT_{ln} (a), heat flow $\dot{Q}$ (b) and overall heat transfer coefficient U (c) plotted over time for experiments with parameter set lowDF (Table 3). Both experiments (RWTH and ISE) are synchronized at the end of the experiment (t=0) when the first tube loses contact to the refrigerant pool. The coefficient of variation *CV* (Eq. (7)) is given in each plot to quantify the deviation between the experiments at RWTH and ISE.

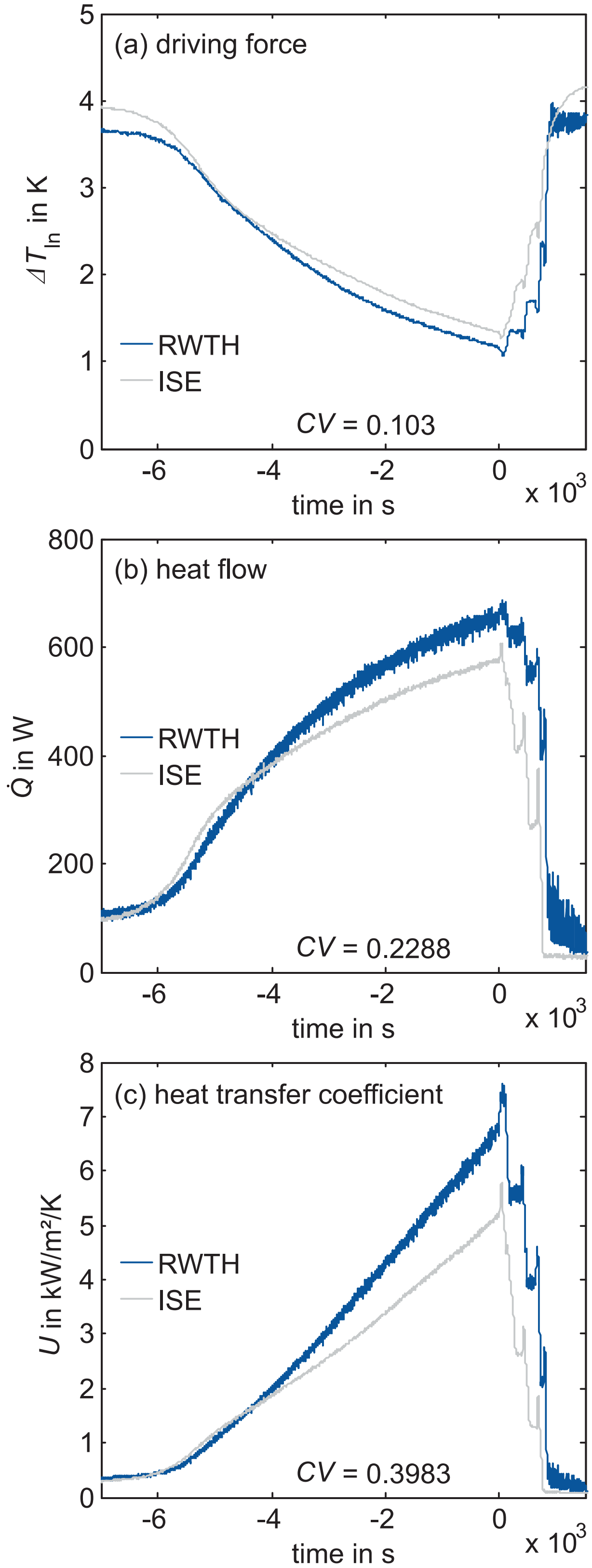

Fig. 5: Driving force ΔT_{ln} (a), heat flow $\dot{Q}$ (b) and overall heat transfer coefficient U (c) plotted over time for experiments with parameter set highDF (Table 3). Both experiments (RWTH and ISE) are synchronized at the end of the experiment (t=0) when the first tube loses contact to the refrigerant pool. The coefficient of variation *CV* (Eq. (7)) is given in each plot to quantify the deviation between the experiments at RWTH and ISE.

The maximum overall heat transfer coefficients reported in literature for comparable thin-film evaporation heat exchangers at similar operating conditions are in the same range, yet slightly lower: Seiler et al. and Lanzerath et al. report values of approx. 5 kW/m²/K in [3,13]. Most likely, the higher U-values in the current work are due to enhanced inner heat transfer of the tubes. Xia et al. investigated tubes with a larger diameter, though the dimensions of the outer structures are similar to the ones examined here. At 15 °C evaporator inlet temperature, approx. 2 K driving force and a relative filling level of 0.5, their reported heat transfer coefficients on the refrigerant side (4 to 5.2 kW/m²/K) are in the same order of magnitude as the overall heat transfer coefficients (U-values) reported here (3 to 5 kW/m²/K) [11]. Since internal heat transfer is not limiting in our case, heat transfer coefficients on the refrigerant side can expected to be only slightly higher than the overall heat transfer coefficients which allows a rough comparison. Thimmaiah et al. also investigated thin-film evaporation on similar tubes, yet they reported overall heat transfer coefficients (U-values) below 1 kW/m²/K at evaporator inlet temperature of 15 °C [15]. In our view, reasons for the lower values are most likely a limitation of the heat transfer on the inner side of the tube and differences in the experimental determination of the driving force ΔT.

3.1.3 Comparison of output quantities

For parameter set lowDF (Table 3), the graphs in Fig. 4 show overall good agreement between measurements at RWTH and ISE: The curve shape of the driving force ΔT_{ln}, heat flow $\dot{Q}$ and U-value for RWTH and ISE are very similar and the values coincide within uncertainty of measurement (SI 6.2).

The values of the driving force ΔT_{ln} in Fig. 4 (a) determined at ISE are most of the time slightly higher than the values measured at RWTH. Consequently, the calculated *CV* is larger than the maximum *CV* calculated for the inlet conditions (< 0.005, Fig. SI7); nevertheless, the correspondence is excellent.

The measured heat flows $\dot{Q}$ in Fig. 4 (b) are almost identical during natural convection of the submerged tubes at the beginning of the experiment. However, starting with the onset of thin-film evaporation, the heat flow $\dot{Q}$ measured at RWTH is slightly higher than at ISE. Furthermore, the random noise is more pronounced in the experimental setup at RWTH (Fig. 4 and Fig. 5) which is due to stronger fluctuations in the evaporator inlet conditions (Fig. SI7) and higher uncertainty of the volume flow sensor at RWTH. The deviations between RWTH and ISE are reflected in a higher *CV* of the heat flows $\dot{Q}$ compared to the *CV* of the driving force ΔT_{ln}.

The U-values of thin-film evaporation determined at RWTH in Fig. 4 (c) are slightly higher throughout the experiment. However, the U-values coincide within uncertainty of measurement with the U-values obtained at ISE (SI 6.2). Maximum and minimum U-values are almost identical (deviation <4%). The *CV* increases compared to the *CV* of the heat flows and logarithmic temperature difference, but is still comparably low.

The experiments with parameter set lowDF show that obtaining comparable results at different experimental setups is possible for thin-film evaporation experiments. For parameter set lowDF, the influence of the experimental setup seems to be small, since the determined values coincide well within uncertainty of measurement.

For parameter set highDF (Table 3), the graphs in Fig. 5 are again similar but show overall less agreement than the graphs for parameter set lowDF: The curve shape of the driving force ΔT_{ln} and heat flow $\dot{Q}$ deviate between RWTH and ISE, though the curve shape of the U-value still appears linear for both setups.

The driving forces ΔT_{ln} at detachment resulting from parameter set highDF are considerably larger than for parameter set lowDF: 1.25 K vs 0.4 K. The minimum and maximum values of the driving force ΔT_{ln} are in good agreement (Fig. 5 (a)) although they do not coincide within the uncertainty of measurement (SI 6.2). Thus, the *CV* is larger than the maximum *CV* of the input conditions (< 0.02, Fig. SI7) and larger than the respective *CV* for parameter set lowDF.

The heat flows $\dot{Q}$ increase compared to parameter set lowDF (maximum values in the range of 600 W vs. 200 W) due to higher exerted driving forces ΔT_{ln}. As for parameter set lowDF, the minimum values of the heat flow $\dot{Q}$ during natural convection of submerged tubes are in good agreement between both setups. However, as the curve shape changes, the increase in heat flow $\dot{Q}$ flattens for ISE compared to

RWTH. Thus, the maximum heat flow $\dot{Q}$ differs: 650 W (RWTH) vs. 580 W (ISE). The deviation of about 11 % is not within the uncertainty of measurement and leads to an increased *CV* compared to the *CV* of the driving force $\Delta T_{\ln}$ and results for parameter set lowDF.

The U-values for natural convection of the submerged tubes are also in good agreement. However, the U-value increases more strongly over time at RWTH than at ISE. As a consequence, the maximum U-values differ: 6.8 kW/m²/K (RWTH) vs. 5.2 kW/m²/K (ISE). The deviation of 24 % is not within uncertainty of measurement and is reflected in a strongly increased *CV* compared to the *CV* of the driving force $\Delta T_{\ln}$ and heat flow $\dot{Q}$ as well as the respective results for parameter set lowDF.

Comparing the results of the measured U-values at RWTH and ISE for the parameter sets lowDF and highDF, it becomes apparent that at low driving force (parameter set lowDF) the results match very well while at higher driving force (parameter set highDF) the results deviate to a greater extent. Furthermore, the measured U-values at RWTH do not show a significant dependence on driving force (maximum U-values 6.5 and 6.8 kW/m²/K for parameter sets lowDF and highDF) whereas ISE results do suggest such a dependence (maximum U-values 6.1 and 5.2 kW/m²/K for parameter sets lowDF and highDF). This outcome indicates that the presence of a driving force impact might depend on the process conditions.

In the following paragraphs the three most plausible explanations for the observed deviations between RWTH and ISE results are discussed. Further potential influencing factors – which are considered as generally important but not responsible for the deviations in our case – are pointed out in detail in the supplementary information.

(1) ***Surface properties***: Literature has shown that thin-film evaporation strongly depends on the surface properties of the heat exchanger: Surface morphology (e.g. roughness), chemistry (e.g. oxidation state), physics (e.g. polarization) and contamination influence wettability [28–30] which is crucial for evaporation [31–33]. Prior to our measurements, we tried to provide identical surface conditions by removing contaminants with an isopropanol cleaning process. However, soldering of the "U"-bend connectors to the finned tubes might have involuntarily modified the surface of the heat exchanger for the ISE setup, e.g. by oxidation due to exposure to high temperatures or contamination with solder or flux agent residuals. Also, exposure to different surrounding media during storage and installation (water vapour, air, gaseous contaminants) might have changed surface conditions. Since thin-film evaporation can be very sensitive to wetting behaviour, we consider differences in surface conditions as a very likely reason for the differences in the measured heat transfer coefficients: Possibly, wettability of the ISE heat exchanger was deteriorated by the soldering process to such an extent that capillary forces did no longer suffice to completely fill the space between the fins at lower filling levels and a partial dry-out occurred. This hypothesis would match the observation that U-values from RWTH and ISE deviate only at higher driving forces where partial dry-out of the tube surface becomes more likely due to higher evaporation mass flow.

(2) ***Configuration of refrigerant pool***: At RWTH, the refrigerant pool has a large volume and it is in direct contact with the evaporator chamber walls, while at ISE the volume is smaller and it is located inside the acrylic glass trough inside the chamber. Thus, at RWTH, the pool has a higher heat capacity and higher heat gains from the ambient can be expected. The energy balance is not assumed to be considerably falsified by this fact since a correction for heat gains was conducted as described in chapter 2.3. However, due to lower heat gains and heat capacity at ISE, evaporation from the pool surface supposedly leads to lower temperatures of the refrigerant pool at ISE compared to RWTH. Thus, the physical properties of the refrigerant are different which could decrease the mass flow through capillary action and therefore explain the lower U-values.

(3) ***Measurement uncertainties:*** For analysing measurement uncertainties, we used accuracy specifications of the manufacturers' datasheets for the pressure and volume flow sensors and calibrated the temperature sensors. We also included uncertainties of the data acquisition systems (see Table 2 and subsection 2.4). However, there might be unforeseen contributions to uncertainty or systematic effects (such as drift effects) which are not included in the

uncertainty analysis. Consequently, the discrepancies between the measurement results from the two different experimental setups might to some extent be due to unknown uncertainties and/or distorting effects.

3.2 Impact of dynamic effects: constant vs. continuously decreasing filling level

In the comparison of experimental setups (Fig. 4 and Fig. 5), the filling level continuously decreased since the refrigerant evaporated but no liquid flowed back from the condenser to the evaporator (Fig. SI13 and Fig. SI14). Thus, each experiment allowed to evaluate all filling levels (1.2 > f_{rel} > -0.25). However, the advantage of evaluating all filling levels within one experiment comes at the price of not having truly steady-state conditions during the experiment. To assess the difference of these "quasi-steady-state conditions" [13] compared to ideal steady-state conditions, we conducted additional experiments using the mobile level drain for liquid reflux (Fig. 2 (b)) to create constant filling levels in the experimental setup at RWTH.

We conducted experiments with evaporator inlet conditions according to Table 4 and a condenser inlet temperature of 10 °C with both continuously decreasing filling level and 6 constant filling levels. Both types of experiments were repeated at least 3 times and the measured U-values are given in Fig. 6.

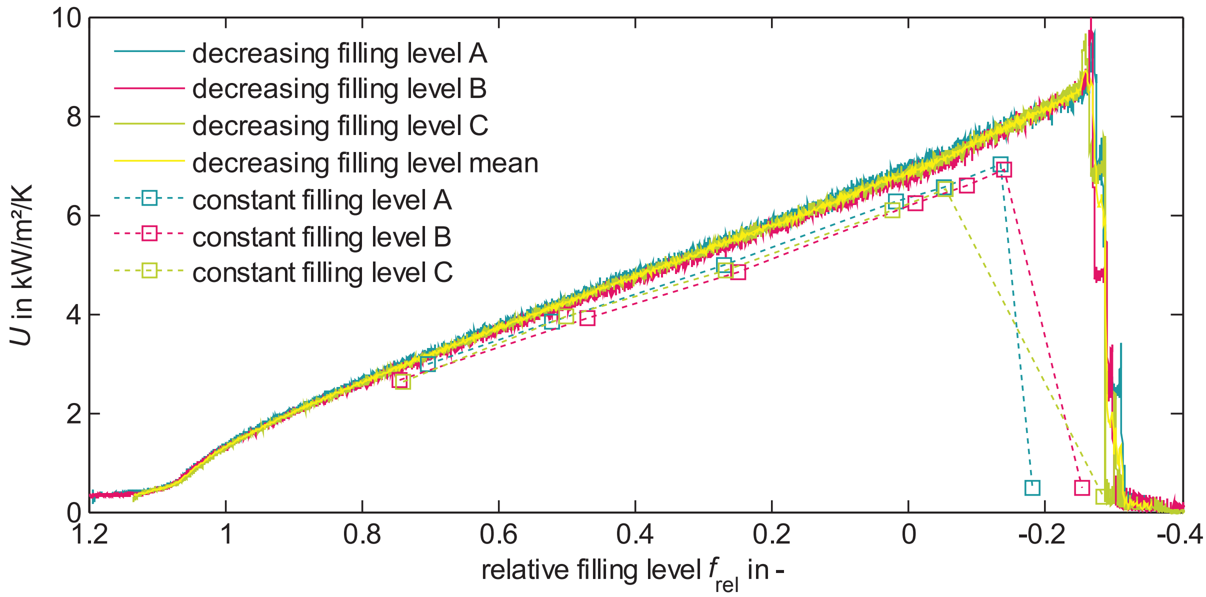

Fig. 6: U-values for experiments with continuously decreasing filling level (for each repetition A-C and arithmetic mean of A-C) and constant filling level (for each repetition A-C) plotted over relative filling level f_{rel}. Operating conditions of evaporator were according to Table 4. Condenser temperature was set to 10 °C. Data points of experiments with constant filling levels are connected by a dashed line to mark subsequently recorded data points.

In Fig. 6, the repetitions of both types of experiments are in very good agreement. Furthermore, both types of experiments show the same trend. Therefore, experiments with continuously decreasing filling levels are well-suited for a quick assessment of the U-value at all filling levels.

However, all experiments with continuously decreasing filling levels lose contact to the refrigerant at lower filling levels and show generally 5-10 % higher U-values than the experiments with constant filling levels. Although the differences are close to or within the uncertainty of measurement, the good reproducibility of the experiments indicates that there are underlying systematic reasons for the decrease in U-value. Possible reasons can be:

(1) Differences in measurement conditions due to measurement uncertainty.
Since the observed differences for experiments with continuously decreasing and constant filling levels are close to or within the uncertainty of measurement, ensuring identical inlet

conditions is crucial. For the shown experiments, the inlet conditions are identical within the uncertainty of measurement, yet still not exactly the same. However, the remaining differences cannot be eliminated in the current experimental setup. Furthermore, the uncertainty of detecting the filling level is difficult to determine but also affects the comparison of the experiments.

(2) Physical effects as discussed in literature. Theoretical and experimental analysis of the thin-film evaporation process suggests that a large share of the evaporation takes place at a rather small region in the vicinity of the 3-phase contact line where refrigerant vapour, liquid and the metal of the heat exchanger meet. In this region, the refrigerant film on the heat exchanger is comparably thin, yet sufficiently thick that intermolecular forces do not prevent evaporation ("disjoining pressure") [11,17,34,35]. This region is affected by the curvature of the liquid-vapour interface and the apparent contact angle between the refrigerant and the heat exchanger. The contact angle, however, is not fixed as its hysteresis ranges from receding (minimum) over equilibrium to advancing (maximum) contact angle [36] and can additionally be affected by dynamics of the liquid [37]. In fact, in the experiments with continuously decreasing filling level, the refrigerant pool level is moving downwards. Thus, the 3-phase contact line that is formed between the tubes, the vapour and the refrigerant pool is also moving. Although the maximum speed of that specific 3-phase contact line is very slow with about 20 mm/h, the movement itself might be sufficient to alter the contact angle and thus be partly responsible for the difference in measured U-values compared to the experiments with constant filling levels.

    A difference in contact angle and, thus, capillary action, could also be the reason for the early detachment of the refrigerant from the tube in case of constant filling levels compared to continuously decreasing filling levels (Fig. 6). However, the measured relative filling levels f_{rel} after detachment have to be considered with caution as the filling level will increase after detachment due to the volume of the detached meniscus that connected the refrigerant and the tube.

4 Conclusion

The first objective of this work was to identify and discuss potential impacts from experimental setups and procedures on the measurement of sub-atmospheric thin-film evaporation of water. To our knowledge, this was the first time that such a comparison has been conducted. Experimental results showed generally good agreement of the evaporation process. For lower driving forces, results from RWTH and ISE, e.g. logarithmic mean temperature differences, heat flows and U-values, are identical within uncertainty of measurement. Experiments with higher driving forces also showed generally good agreement of the curve shapes for the evaluated evaporation quantities, yet revealed deviations in absolute U-value of up to 24 %. We believe that this discrepancy is most likely caused by different surface properties of the heat exchangers and remaining systematic differences between the measurement setups.

Based on our findings, we conclude that thin-film evaporation measurements can generally yield comparable results from different experimental setups. However, there are many parameters associated with the setup and procedure which are prone to be overlooked and which – if disregarded – can easily render a comparison of measurement results invalid. In particular, we consider the following aspects as very important:

The analysis of measurement uncertainties is crucial since small uncertainties can lead to larger uncertainties in calculated quantities due to propagation of uncertainties. In this work, the combination of high heat flows in the evaporator at small driving forces leads to small temperature differences between in- and outlet temperature of the fluid and between fluid and saturation

temperature. As a result, even the rather small uncertainties of the temperature and pressure sensors can have a very large effect on the propagated uncertainties of the temperature differences.
For comparison of experiments, their input conditions need to be identical and if possible constant. This refers to evaporator inlet temperature, volume flow and evaporation temperature (saturation pressure in the evaporator).
For capillary assisted thin-film evaporators, the exact definition of the investigated heat exchanger's surface properties need to be provided as they can have a crucial effect on wetting behaviour, capillary action and consequently on evaporation performance. It should be taken into account that the manufacturing process, storage and measurement conditions can change the surface properties. In order to contribute to the creation of correlations, it would be valuable to provide contact angles for the investigated finned copper tubes at process conditions present during the experiments in future works. More information regarding contact angles can be found in the supplementary information (SI 6.5).
In general, control of non-condensable gases is a major challenge for evaporation experiments in sub-atmospheric pressure conditions. Non-condensable gases can distort the measurement of saturation pressure, impede condensation and possibly influence evaporation mechanisms. Therefore, vacuum tightness of the system and knowledge or control of leak rates are essential for reproducible experimental results.
The second objective of this work was to assess the impact of filling level dynamics: For the first time, we compared measurements at decreasing filling levels with experiments at constant filling levels. Results show that experiments with continuously decreasing filling level are well-suited for quickly characterising heat exchangers at all filling levels. However, for decreasing filling levels, measured U-values were always 5-10 % higher. Although the differences are close to or within uncertainty of measurement, excellent reproducibility of the experiments suggest that there are underlying systematic reasons. This effect could even be exploited in future thin-film evaporators: Instead of evaporating at a constant filling level with continuous reflux, the evaporator could be operated with decreasing filling level and quick intermittent refills. Thereby, the maximum achievable U-value would increase by up to 10 %.
From our experience, we conclude that comparing absolute values obtained from different experimental setups requires a detailed look at experimental setup and conditions. Unfortunately, the required information is not always completely provided in literature. However, if all relevant influencing factors are considered in measurement conduction and evaluation, reasonable comparisons are possible.

5 Acknowledgement

We thank Wieland Werke AG for providing the heat exchanger tubes. RWTH Aachen and Fraunhofer ISE gratefully acknowledge the financial support from the German Federal Ministry for Economic Affairs and Energy (BMWi) in the "7th Energy Research Programme of the Federal Government" (03EN2002A & 03EN2012A). The work at Fraunhofer ISE was supported by Fraunhofer Zukunftsstiftung in the context of the project HArVest.

6 Supplementary Information

6.1 Input conditions for experiments

In order to be able to compare the results of the experimental setups at RWTH and ISE, the input conditions of the experiments need to be as similar as possible. The input conditions (volume flow, inlet temperature and evaporator pressure) are given in Fig. SI7 for parameter set lowDF (corresponding to Fig. 4) and Fig. SI8 for parameter set highDF (corresponding to Fig. 5).

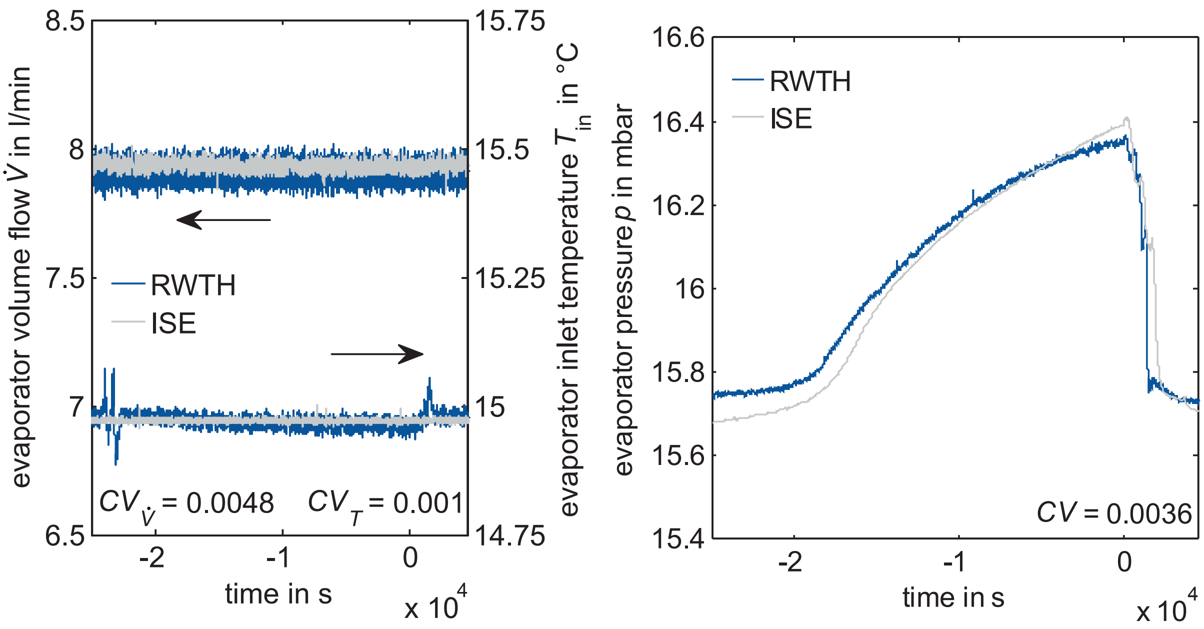

Fig. SI7: Operating conditions for experiments with parameter set lowDF plotted over time. Left: evaporator volume flow $\dot{V}$ and inlet temperature T_{in}, right: evaporator pressure p. Both experiments (RWTH and ISE) are synchronized at the end of the experiment (t=0) when the first tube loses contact to the refrigerant pool.

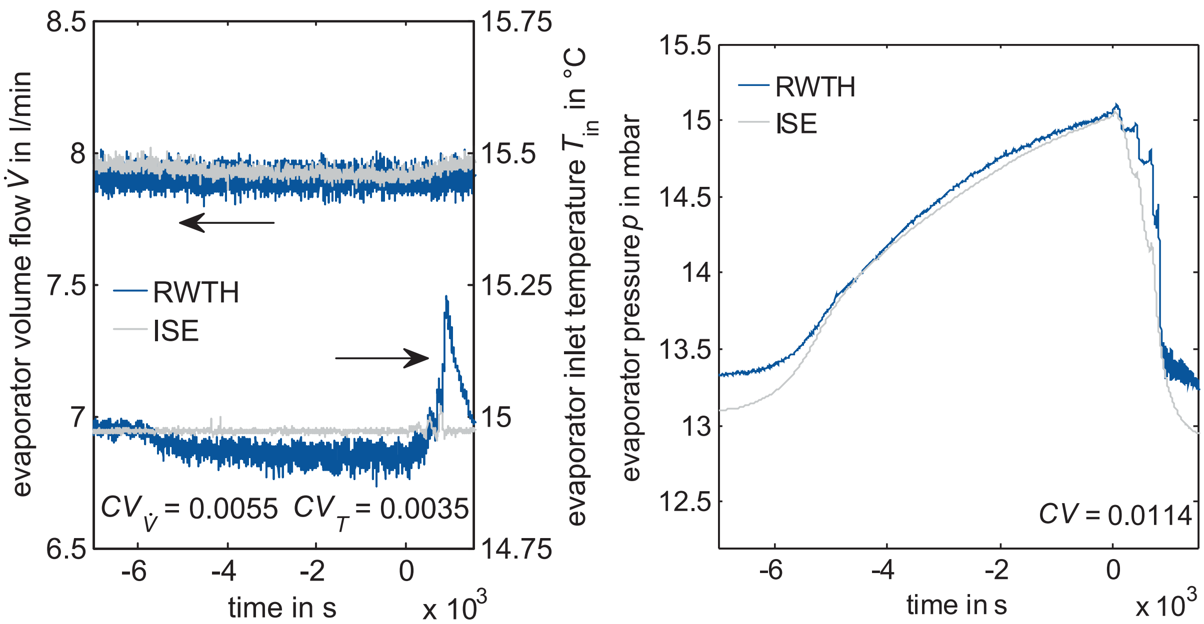

Fig. SI8: Operating conditions for experiments with parameter set highDF plotted over time. Left: evaporator volume flow $\dot{V}$ and inlet temperature T_{in}, right: evaporator pressure p. Both experiments

(RWTH and ISE) are synchronized at the end of the experiment (t=0) when the first tube loses contact to the refrigerant pool.

During thin-film evaporation until the contact between the tubes and the water is lost, the input conditions of the presented experiments show good agreement within uncertainty of measurement in both experimental setups. This results in very low *CV*s given in Fig. SI7 and Fig. SI8.
The evaporator volume flow and inlet temperature are constant and almost identical for both setups (left in Fig. SI7 and Fig. SI8). However, the inlet temperature of the RWTH setup shows peaks at the beginning and the end of the evaporation process for both parameter sets due insufficient control of the thermostat. Nevertheless, these peaks do not affect the experiments as they do not occur during the relevant thin-film evaporation. Furthermore, the inlet temperature of the RWTH setup is slightly lower for the parameter set highDF once the thin-film evaporation started, since the thermostat was not able to keep the temperature constant. We repeated the experiment with slightly higher inlet temperatures in the RWTH setup and obtained no considerable differences. Thus, the difference in inlet temperature can be neglected.
The measured evaporation pressure shows similar curve shapes and almost identical maximum and minimum values. Although the measured values are not identical, their values coincide within the uncertainty of measurement. The measured pressures are not constant during the experiment as they adapt to the current UA values of the evaporator and condenser since the fluid inlet temperatures of both components are set.

6.2 Uncertainty in measurement

The uncertainty of measurement for all calculated quantities plotted in Fig. 4 and Fig. 5 are given in Fig. SI9 and Fig. SI11. The uncertainties were calculated using equation (6) and sensor uncertainties given in Table 2 according to the “Guide to the expression of uncertainty in measurement” (GUM) using a coverage factor of k = 1 [27]. In Fig. SI10 and Fig. SI12, the uncertainty of measurement is plotted as background behind the actually measured values given in Fig. 4 and Fig. 5. The used colours in Fig. SI10 and Fig. SI12 differ from the colours in Fig. 4 and Fig. 5 to improve readability of the uncertainty range.

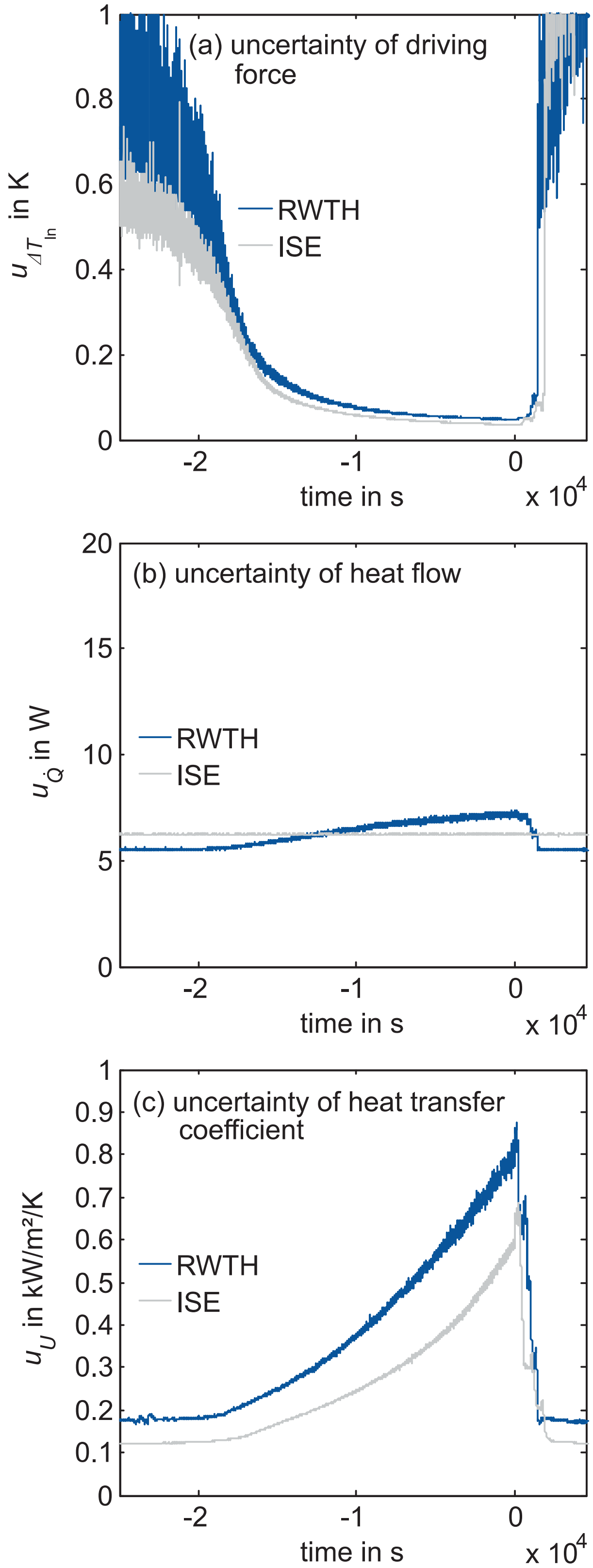

Fig. SI9: Uncertainty in measurement for the quantities driving force ΔT_{ln} (a), heat flow $\dot{Q}$ (b) and heat transfer coefficient U (c) shown in Fig. 4 for experiments with parameter set lowDF plotted over time. Both experiments (RWTH and ISE) are synchronized at the end of the experiment (t=0) when the first tube loses contact to the refrigerant pool.

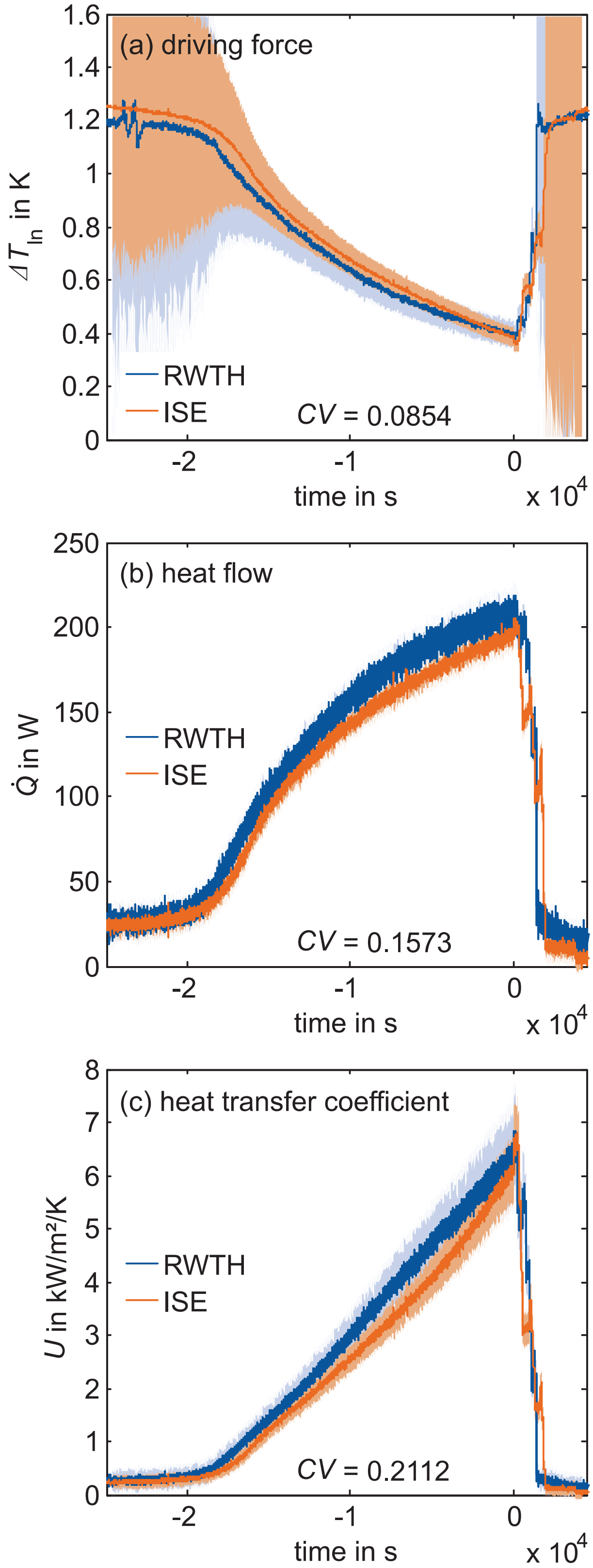

Fig. SI10: driving force $\Delta T_{\ln}$ (a), heat flow $\dot{Q}$ (b) and heat transfer coefficient U (c) shown in Fig. 4 together with uncertainties of measurement (shown in Fig. SI9) in background for experiments with parameter set lowDF plotted over time. Both experiments (RWTH and ISE) are synchronized at the end of the experiment (t=0) when the first tube loses contact to the refrigerant pool.

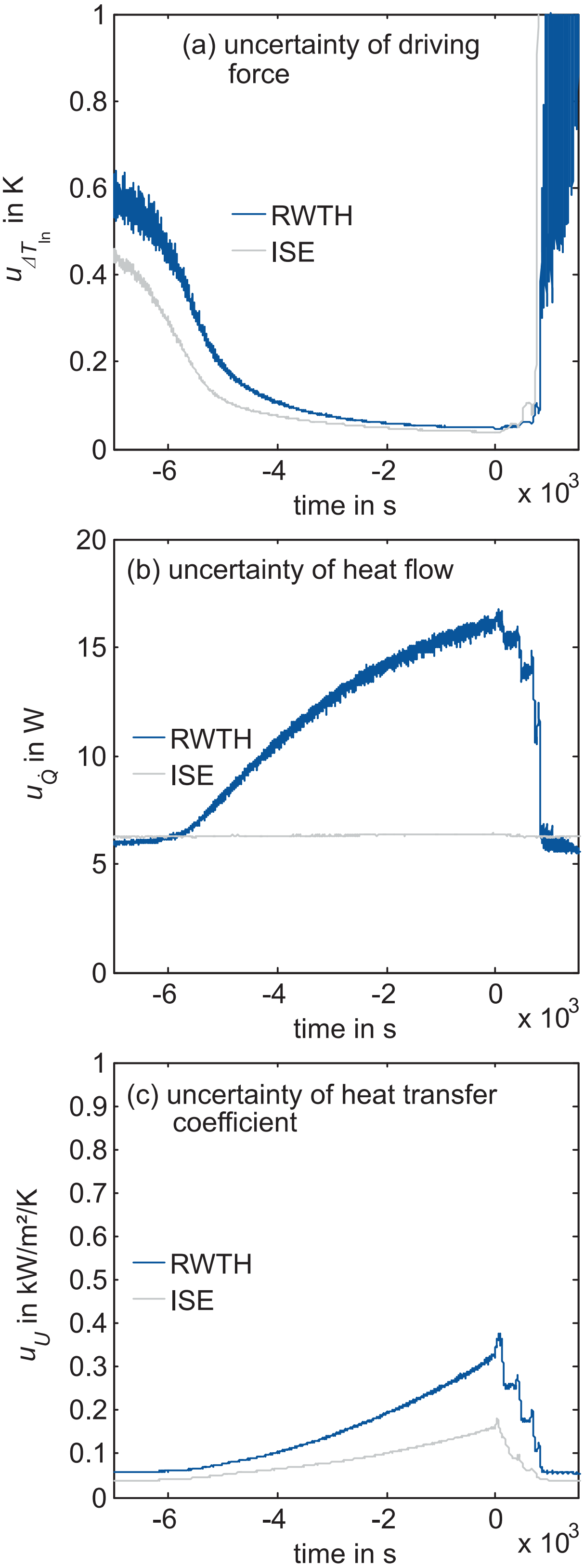

Fig. SI11: Uncertainty in measurement for the quantities driving force ΔT_{ln} (a), heat flow $\dot{Q}$ (b) and heat transfer coefficient U (c) shown in Fig. 5 for experiments with parameter set highDF plotted over time. Both experiments (RWTH and ISE) are synchronized at the end of the experiment (t=0) when the first tube loses contact to the refrigerant pool.

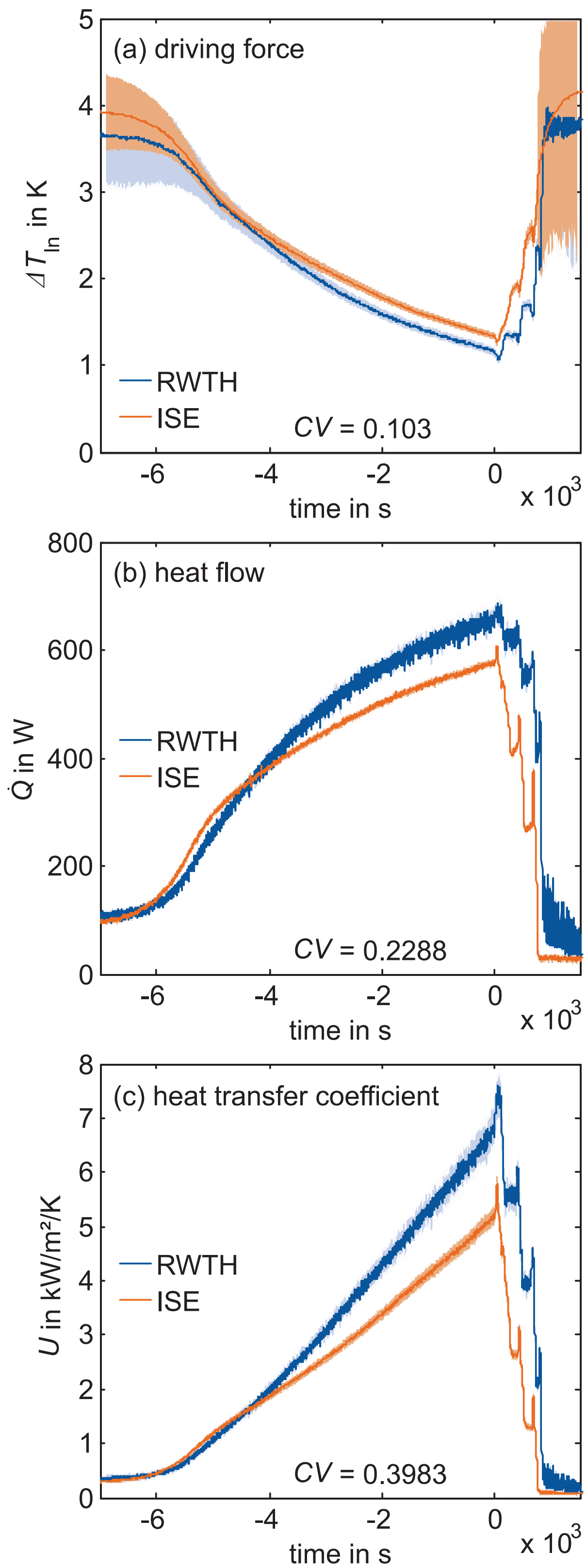

Fig. SI12: Driving force ΔT_{ln} (a), heat flow $\dot{Q}$ (b) and heat transfer coefficient U (c) shown in Fig. 5 together with uncertainties of measurement (shown in Fig. SI11) in background for experiments with parameter set highDF plotted over time. Both experiments (RWTH and ISE) are synchronized at the end of the experiment (t=0) when the first tube loses contact to the refrigerant pool.

6.3 Discussion of other potential reasons for observed deviations between RWTH and ISE

The three aspects that we consider most likely to be responsible for the discrepancies in the measurement results from RWTH and ISE are discussed in detail in chapter 3.1. Further factors which might generally influence evaporation measurements but which are considered negligible in our case are pointed out in detail below:

4. ***Heat exchanger design:*** While at RWTH evaporation can only take place at the finned tube sections, at ISE also connecting plain tube sections and the "U"-bends are in contact with refrigerant and can potentially contribute to evaporation. However, refrigerant which was condensed on the plain tube sections above the pool surface evaporated completely before the evaluated time interval. Thus, results cannot be affected by the additional evaporation source. The plain "U"-bends are immersed in the refrigerant pool and form contact lines, but the contact line length is very small compared to the contact line length of the finned tube section. Therefore, a noticeable impact on the measurement is not expected.
5. ***Tube alignment***: Ideally, the evaporator tubes should be aligned perfectly horizontal to achieve a homogeneous refrigerant distribution in the fins interstices and a synchronous detachment of the refrigerant meniscus at the end of the experiment. If the tubes are slightly tilted, altered and undefined wetting conditions could change evaporation power and U-values. The ISE setup is generally more susceptible to improper tube alignment since the heat exchanger is not mechanically fixed in its place except the hose connections. However, measured U-values should show an extended period of time for detachment if the tubes were imprecisely aligned. As this period of time is very similar at RWTH and ISE, the precision of tube alignment is not considered as possible reason for the deviations in the presented measurements.
6. ***Constructional conditions for vapour flow***: Number, geometry and arrangement of connection lines and valves between evaporator and condenser can induce a pressure drop and determine fluid flow dynamics. Since the system pressure is measured directly inside the evaporator chamber, pressure drops in the connection to the condenser cannot distort the results in the evaporator. The vacuum chambers have a rather large and open volume so that a homogeneous pressure distribution within them is assumed. Vapour flow dynamics inside the evaporator chamber are considered to be negligible for the pressure measurement since applied driving forces and thereby vapour velocities at the location of the pressure sensors are small.
7. ***Pressure difference***: A process-related factor, which should be considered in the interpretation of the results, is the slight difference in pressure between RWTH and ISE measurements (see Fig. SI7 and Fig. SI8). Since neither of the two setups can directly control pressure, the pressure in the evaporator chamber is rather an output quantity which dynamically adapts to fluid temperatures, volume flows and heat transfer capabilities of the evaporator and condenser. The resulting maximum pressure difference occurred in the flooded period and was approx. 0.1 mbar for parameter set lowDF and approx. 0.3 mbar for parameter set highDF. During the second half of the partially flooded period – in which the largest differences of U and $\dot{Q}$ between RWTH and ISE results appear – the pressure difference was only approx. 0.05 mbar (parameter set lowDF) and 0.1 mbar (parameter set highDF). This rather small difference is within the uncertainty of measurement of the pressure sensors and therefore, we consider it as not sufficient for having a remarkable effect on the refrigerant's material properties and thus do not take this factor into account as a reason for the measured differences.

8. ***Non-condensable gases***:
Since the calculation of saturation temperature from the absolute pressure signal is based on the assumption of a pure water atmosphere, the presence of non-condensable gases inside the evaporator chamber would distort this calculation. Generally, a certain leakage of gaseous compounds from the environment to the interior cannot be avoided with any vacuum system and must be expected in both setups. However, non-condensable gases can enter the vacuum also in a different way: Our observations indicate that during exposure to air, gaseous components are adsorbed on the heat exchanger surface and/or dissolved in the refrigerant. After exposition to vacuum, the gaseous components are not directly released which can lead to significant deviations of the first measurements after installation compared to the subsequent ones. Consequently, measurement results are only dependable if a series of reproduction measurements do not show any significant changes anymore.
To control leakage of non-condensable gases inside the vacuum chamber, evacuation procedures are necessary. While at RWTH non-condensables were constantly withdrawn from the system, evacuation at ISE only took place before the refrigerant was condensed on the evaporator. Thus, it can be assumed that the ISE evacuation procedure leads to higher partial pressures of non-condensable gases than the RWTH procedure. However, quantification of the partial pressures is not possible at either of the two setups.
Besides quantity, the distribution of non-condensable gases within the closed system is an important issue: Supposing that the non-condensable gases were equally distributed within the system, they would massively falsify the calculated saturation temperature. However, in a closed evaporator-condenser system, non-condensable gases usually accumulate at the place of condensation [38]. Therefore, it can be assumed that only a minor fraction of the non-condensable gases remain in the evaporator and distort the pressure signal. This statement is supported by additional measurements at ISE with intermittent evacuation phases during evaporation which did not yield considerably different results in the heat transfer coefficient. Despite the lack of knowledge of the exact amount of non-condensable gases inside the evaporators, this factor can definitely not be the cause for the difference in U-values between RWTH and ISE: If non-condensable gases distorted the pressure signal at ISE, the corrected saturation temperature would be lower than the evaluated one which would – according to equations (1) and (4) – result in a higher driving force and a lower U-value. Since the calculated U-values of the ISE measurements are already lower than of RWTH, a correction for non-condensable gases would rather increase the differences than diminish them. However, the presence of non-condensable gases can affect the conclusions drawn on the impact of driving force: Given that the measurement duration of parameter set lowDF was about four times as long as of parameter set highDF a considerably greater amount of non-condensable gases can be assumed for parameter set lowDF for the ISE measurements. Consequently – if non-condensables play a relevant role at all – a reduction of U-values would affect parameter set lowDF much stronger than parameter set highDF. The two U curves from ISE would then come closer together and the concluded effect of driving force on heat transfer coefficient would lessen.

6.4 Relative filling level f_{rel} detected optically in experimental setup at RWTH

The optically detected relative filling levels f_{rel} in the experimental setup at RWTH are given in Fig. SI13 for parameter set lowDF and in Fig. SI14 for parameter set highDF. Details on the optical detection system can be found in Fig. 2 (c) and subsection 2.2.1.

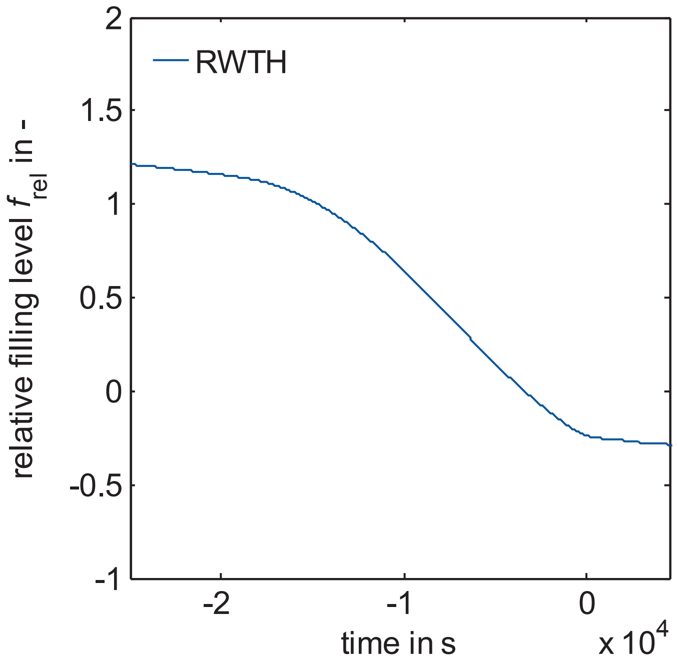

Fig. SI13: Relative filling level f_{rel} detected optically in the experimental setup at RWTH for the experiment with parameter set lowDF shown in Fig. 4.

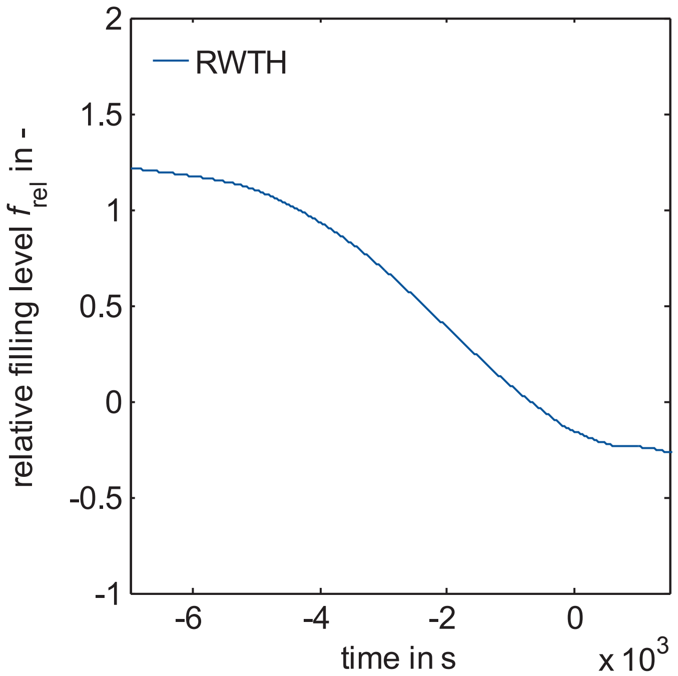

Fig. SI14: Relative filling level f_{rel} detected optically in the experimental setup at RWTH for the experiment with parameter set highDF shown in Fig. 5.

6.5 Contact angle

Unfortunately, we are unable to determine the wetting angle on the surface of the heat exchanger's fins (material Cu, C12200) at the process conditions of the experiments. Evaluating pictures taken from the side of the experimental setup at RWTH (cf. Fig. 1) gives a hint on contact angle and indicates that it changes at different process conditions, yet the quality and resolution of the pictures impede proper quantitative assessment. The height of the water meniscus between the fins at process conditions is also difficult to determine through the existing windows. The space between the fins is usually almost completely filled with refrigerant, although the picture in Fig. 1 reveals differences in the height of the meniscus between different fins. Zooming in on the picture in Fig. 1 shows that on the upper end of the tube´s fins, the distance between the highest point of refrigerant and the lowest point of the refrigerant in the middle between two fins is usually smaller than the fin width (0.15 mm) in the picture. However, evaluation of distances in this picture can be prone to large errors due to resolution and sharpness of the picture as well as slight perspective deviation.

7 References

[1] F. Giraud, R. Rullière, C. Toublanc, M. Clausse, J. Bonjour, Experimental evidence of a new regime for boiling of water at subatmospheric pressure, Exp. Therm. Fluid Sci. 60 (2015) 45–53.

[2] F. Giraud, C. Toublanc, R. Rullière, J. Bonjour, M. Clausse, Experimental study of water vaporization occurring inside a channel of a smooth plate-type heat exchanger at subatmospheric pressure, Appl. Therm. Eng. 106 (2016) 180–191.

[3] J. Seiler, F. Lanzerath, C. Jansen, A. Bardow, Only a wet tube is a good tube: understanding capillary-assisted thin-film evaporation of water for adsorption chillers, Appl. Therm. Eng. 147 (2019) 571–578.

[4] G. Ribatski, A.M. Jacobi, Falling-film evaporation on horizontal tubes—a critical review, Int. J. Refrig. 28 (2005) 635–653.

[5] B. Narváez-Romo, M. Chhay, E.W. Zavaleta-Aguilar, J.R. Simões-Moreira, A critical review of heat and mass transfer correlations for LiBr-H 2 O and NH 3 -H 2 O absorption refrigeration machines using falling liquid film technology, Appl. Therm. Eng. 123 (2017) 1079–1095.

[6] R. Volmer, J. Eckert, G. Füldner, L. Schnabel, Evaporator development for adsorption heat transformation devices – Influencing factors on non-stationary evaporation with tube-fin heat exchangers at sub-atmospheric pressure, Renew. Energy 110 (2017) 141–153.

[7] R. Volmer, T. Schalling, L. Schnabel, Vermessung des dynamischen Verdampfungs- und Kondensationsverhaltens an Wärmeübertragern für adsorptionstechnische Anlagen, in: DKV-Tagungsbericht 2014 Düsseldorf, 19. - 21. November 2014.

[8] R. Volmer, J. Eckert, L. Schnabel, Analyse geometrischer Einflussfaktoren auf die Niederdruckverdampfung von Wasser an Lamellenwärmeübertragern, in: DKV-Tagungsbericht 2015 Dresden, 18. - 20. November 2015.

[9] A. Warlo, H. Seifarth, R. Volmer, L. Schnabel, Evaluation of innovative heat exchanger designs and operation modes for the subatmospheric evaporation of water, in: ISHPC 2017 Proceedings, 2017.

[10] L. Schnabel, R. Volmer, A. Warlo, P. Schossig, Evaluation of Different Evaporator Designs and Concepts for Sorption Processes Using Water as Refrigerant, in: International Institute of Refrigeration (Ed.), 13th IIR-Gustav Lorentzen Conference on Natural Refrigerants Proceedings: Natural refrigerant solutions for warm climate countries, 2018.

[11] Z.Z. Xia, G.Z. Yang, R.Z. Wang, Experimental investigation of capillary-assisted evaporation on the outside surface of horizontal tubes, Int. J. Heat Mass Transf. 51 (2008) 4047–4054.

[12] L. Schnabel, K. Witte, J. Kowol, P. Schossig, Evaluation of different evaporator concepts for thermally driven Sorption Heat Pumps and Chillers, in: ISHPC 2011 Proceedings, 2011, pp. 543–552.
[13] F. Lanzerath, J. Seiler, M. Erdogan, H. Schreiber, M. Steinhilber, A. Bardow, The impact of filling level resolved: Capillary-assisted evaporation of water for adsorption heat pumps, Appl. Therm. Eng. (2016) 513–519.
[14] R. Volmer, N. Alario, J. Weise, O. Andersen, L. Schnabel, Two Approaches for Enhanced Evaporation of Water at Subatmospheric Pressure., in: ISHPC 2017 Proceedings, 2017.
[15] P.C. Thimmaiah, A. Sharafian, W. Huttema, C. Osterman, A. Ismail, A. Dhillon, M. Bahrami, Performance of finned tubes used in low-pressure capillary-assisted evaporator of adsorption cooling system, Appl. Therm. Eng. 106 (2016) 371–380.
[16] C.-Y. Wang, C.-J. Tu, Effects of non-condensable gas on laminar film condensation in a vertical tube, Int. J. Heat Mass Transf. 31 (1988) 2339–2345.
[17] F. Crößmann, Untersuchung der Verdampfung aus strukturierten Oberflächen in Reinstoffatmosphäre. PhD thesis, Darmstadt, 2016.
[18] C. Schulze, A Contribution to Numerically Efficient Modelling of Thermodynamic Systems. PhD thesis, Braunschweig, 2013.
[19] E.W. Lemmon, M.O. McLinden, D.G. Friend, Thermopyhsical properties of fluid systems, in: P.J. Lindstrom, W.G. Mallard (Eds.), NIST Standard Reference Database, Gaithersburg, MD 20899, 2013.
[20] W. Wagner, A. Pruß, The IAPWS Formulation 1995 for the Thermodynamic Properties of Ordinary Water Substance for General and Scientific Use, J. Phys. Chem. Ref. Data 31 (2002) 387–535.
[21] J.D. Cox, D.D. Wagman, V.A. Medvedev, CODATA Key Values for Thermodynamics, Hemisphere Publishing Corp, New York, 1989.
[22] M.W. Chase Jr., NIST-JANAF Themochemical Tables, 4th ed., J. Phys. Chem. Ref. Data Monograph, 1998.
[23] L.A. Guildner, D.P. Johnson, F.E. Jones, Vapor pressure of water at its triple point: highly accurate value, Science 191 (1976) 1261.
[24] G.S. Kell, Density, thermal expansivity, and compressibility of liquid water from 0 °C to 150 °C: Correlations and Tables for Atmospheric Pressure and Saturation Reviewed and Expressed on 1968 Temperature Scale, J. Chem. Eng. Data 20 (1975) 97–105.
[25] N.S. Osborne, H.F. Stimson, D.C. Ginnings, Measurements of heat capacity and heat of vaporization of water in the range 0° to 100°C, J. Res. Nat. Bur. Stand. 23 (1939) 197–260.
[26] H.F. Stimson, Some precise measurements of the vapor pressure of water in the range from 25 to 100 °C, J. Res. Natl. Bur. Stand. A Phys. Ch. 73A (1969) 493–496.
[27] Joint Committee for Guides in Metrology (JCGM), Evaluation of measurement data - Guide to the expression of uncertainty in measurement: JCGM 100:2008. GUM 1995 with minor corrections, 2008, http://www.bipm.org/en/publications/guides/gum_print.html, accessed May 25th, 2019.
[28] P.-G. de Gennes, F. Brochard-Wyart, D. Quéré, Capillarity and wetting phenomena: Drops, bubbles, pearls, waves, Springer, New York, NY, 2009.
[29] M. Yekta-fard, A.B. Ponter, Surface Treatment and Its Influence on Contact Angles of Water Drops Residing on Polymers and Metals, Phys. Chem. Liquids 15 (1985) 19–30.
[30] M.R.S. Shirazy, S. Blais, L.G. Fréchette, Mechanism of wettability transition in copper metal foams: From superhydrophilic to hydrophobic, Appl. Surf. Sci. 258 (2012) 6416–6424.

[31] C.Y. Lee, T.H. Chun, W.K. In, Effect of change in surface condition induced by oxidation on transient pool boiling heat transfer of vertical stainless steel and copper rodlets, Int. J. Heat Mass Transf. 79 (2014) 397–407.
[32] K. Yuki, K. Fukushima, A. Takemura, K. Suzuki, Wettability and evaporation enhancement for heat transport devices by high performance oxide layer, in: 2015 International Conference on Electronic Packaging and iMAPS All Asia Conference (ICEP-IAAC), IEEE, 2015, pp. 601–604.
[33] H.-Y. Kim, B.H. Kang, Effects of hydrophilic surface treatment on evaporation heat transfer at the outside wall of horizontal tubes, Appl. Therm. Eng. 23 (2003) 449–458.
[34] S. Fischer, Experimental Investigation of Heat Transfer during Evaporation in the Vicinity of Moving Three-Phase Contact Lines. PhD thesis, Darmstadt, 2015.
[35] M. Potash, P.C. Wayner, Evaporation from a two-dimensional extended meniscus, Int. J. Heat Mass Transf. 15 (1972) 1851–1863.
[36] L. Gao, T.J. McCarthy, How Wenzel and cassie were wrong, Langmuir 23 (2007) 3762–3765.
[37] H.B. Eral, D.J.C.M. 't Mannetje, J.M. Oh, Contact angle hysteresis: a review of fundamentals and applications, Colloid Polym. Sci. 291 (2013) 247–260.
[38] P. van Carey, Liquid Vapor Phase Change Phenomena: An Introduction to the Thermophysics of Vaporization and Condensation Processes in Heat Transfer Equipment, 2nd ed., Chapman and Hall/CRC, Boca Raton, 2018.